Probing the S1/S1′ Substrate Binding Pocket Geometry of HIV-1 Protease with Modified Aspartic Acid Analogues†

Glenn F. Short, III, Andrei L. Laikhter, Michiel Lodder, Yuda Shayo, Tuncer Arslan, and Sidney M. Hecht*

Departments of Chemistry and Biology, University of Virginia, Charlottesville, Virginia 22901

Received February 1, 2000; Revised Manuscript Received April 10, 2000

ABSTRACT: Aspartates 25 and 125, the active site residues of HIV-1 protease, participate functionally in proteolysis by what is believed to be a general acid−general base mechanism. However, the structural role that these residues may play in the formation and maintenance of the neighboring S1/S1′ substrate binding pockets remains largely unstudied. Because the active site aspartic acids are essential for catalysis, alteration of these residues to any other naturally occurring amino acid by conventional site-directed mutagenesis renders the protease inactive, and hence impossible to characterize functionally. To investigate whether Asp-25 and Asp-125 may also play a structural role that influences substrate processing, a series of active site protease mutants has been produced in a cell-free protein synthesizing system via readthrough of mRNA nonsense (UAG) codons by chemically misacylated suppressor tRNAs. The suppressor tRNAs were activated with the unnatural aspartic acid analogues *erythro*-β-methylaspartic acid, *threo*-β-methylaspartic acid, or β,β-dimethylaspartic acid. On the basis of the specific activity measurements of the mutants that were produced, the introduction of the β-methyl moiety was found to alter protease function to varying extents depending upon its orientation. While a β-methyl group in the *erythro* orientation was the least deleterious to the specific activity of the protease, a β-methyl group in the *threo* orientation, present in the modified proteins containing *threo*-β-methylaspartate and β,β-dimethylaspartate, resulted in specific activities between 0 and 45% of that of the wild type depending upon the substrate and the substituted active site position. Titration studies of pH versus specific activity and inactivation studies, using an aspartyl protease specific suicide inhibitor, demonstrated that the mutant proteases maintained bell-shaped pH profiles, as well as suicide-inhibitor susceptibilities that are characteristic of aspartyl proteases. A molecular dynamics simulation of the β-substituted aspartates in position 25 of HIV-1 protease indicated that the *threo*-β-methyl moiety may partially obstruct the adjacent S1′ binding pocket, and also cause reorganization within the pocket, especially with regard to residues Val-82 and Ile-84. This finding, in conjunction with the biochemical studies, suggests that the active site aspartate residues are in proximity to the S1/S1′ binding pocket and may be spatially influenced by the residues presented in these pockets upon substrate binding. It thus seems possible that the catalytic residues cooperatively interact with the residues that constitute the S1/S1′ binding pockets and can be repositioned during substrate binding to orient the active site carboxylates with respect to the scissile amide bond, a process that likely affects the facility of proteolysis.

The maturation of human immunodeficiency virus type-1 (HIV-1) (*1*) requires the participation of the viral enzyme HIV-1 protease (*2*). The aspartyl protease is expressed as part of a *gag-pol* polyprotein precursor that is packaged into immature virions during budding from the cell membrane of the host (*3*). Viral maturation from virion to infectious virus is catalyzed by HIV-1 protease-mediated cleavage of several *gag*-encoded structural proteins, which are important to proper viral assembly, as well as the *pol* gene components reverse transcriptase, integrase, and unprocessed HIV-1 protease, all known to play crucial roles during the viral life cycle (*4*). Mutants of HIV-1 that lack functional HIV-1 protease failed to adequately process the *gag-pol* precursor and resulted in the formation of immature virions and a subsequent loss of viral infectivity (*2*). This result has prompted the exploitation of HIV-1 protease as a therapeutic target for the development of several anti-HIV agents that are currently in clinical use (*5*).

On the basis of both structural and biochemical studies, the active form of HIV-1 protease is known to be a 22 kDa homodimer composed of identical 99-amino acid subunits (*6*−*9*). The monomers of HIV-1 protease dimerize via a four-stranded antiparallel β-sheet involving both the amino and carboxyl termini of each subunit to yield an overall structure with C_2 symmetry. A long, deep cleft is formed at the dimer interface, creating the catalytic center, as well as the substrate binding pocket of the enzyme. Each monomer contributes one active site aspartate residue to the catalytic center and presents the residue within a loop structure that interlocks with its symmetric counterpart by extensive hydrophobic interaction (*7*). The substrate is believed to bind along the length of the cleft by extensive hydrogen bonding with the peptide backbone, as well as van der Waals contacts with the side chains of the substrate (*10*).

† This work was supported by NIH Research Grant CA77359 awarded by the National Cancer Institute.

10.1021/bi000214t CCC: $19.00
Published on Web 07/06/2000

HIV-1 protease substrate specificity has been analyzed through the study of substrate preferences of the enzyme (*10*−*15*), noncleavable enzyme−inhibitor complexes (*16*−*18*), and phenotypic changes resulting from single missense mutations (*19*). HIV-1 protease is known to bind substrate-based inhibitors within its binding cleft in an extended β-sheet conformation to allow interaction with both the peptide backbone and side chains of the inhibitor. The basis of substrate recognition results from interactions between at least six hydrophobic subsites (S3, S2, S1, S1′, S2′, and S3′) lining the walls of the binding cleft and the respective side chains of the substrate (P3, P2, P1, P1′, P2′, and P3′) that extend into these pockets. Because the catalytic mechanism of HIV-1 protease is thought not to involve a covalent intermediate (*20*), the substrate must be anchored rigidly within the binding cleft to ensure facile cleavage of the appropriate amide bond. While two flexible flap regions assist the protease in securing the substrate within the active site cleft, the large number of hydrophobic subsites within the binding cleft allow van der Waals contacts with specific substrate residues on either side of the scissile bond (*10*). In both known classes of HIV-1 protease substrates, substrate specificity has been shown to rely on those hydrophobic subsites closest to the scissile bond (i.e., S1, S1′, S2, and S2′) (*21*).

The S1 and S1′ subsites, which flank the scissile bond of the substrate, are particularly important for efficient substrate recognition and subsequent proteolysis. Structures of inhibitor−enzyme complexes show that the catalytic aspartates may help constitute one face of the S1/S1′ subsites, while Leu-123/Leu-23, Pro-181/Pro-81, Val-182/Val-82, and Ile-184/Ile-84 contribute to the formation of the remainder of the binding pockets (*10*) (Figure 1). Of these residues, only Val-182/Val-82 was found to tolerate small degrees of mutagenic changes, whereas alteration of Leu-123/Leu-23, Asp-125/Asp-25, Pro-181/Pro-81, and Ile-184/Ile-84 to any other amino acid was deleterious to HIV-1 protease activity (*19*). Interestingly, on the basis of empirically derived contributions by each amino acid to the overall free energy of inhibitor binding, the most stable region of the protease includes the same S1/S1′ subsite residues, namely, Asp-25, Pro-81, Val-82, and Ile-84 (*22*). These residues are thought to be in preformed conformations that facilitate the binding of the inhibitor and presumably the substrate. Further, the emergence of HIV-1 protease mutants during chemotherapy, resistant to one or more clinically useful protease inhibitors, has been shown to occur through a series of point mutations of residues in and around the S1/S1′ substrate binding pockets (*23*, *24*). Substitution of Val-82 and Ile-84 tend to be the most prominent viral mutations that lead to HIV resistance (*23*−*26*) and suggest the importance of the S1/S1′ subsite geometries during inhibitor, and hence substrate recognition.

Structures of inhibitor−enzyme complexes implicate the catalytic aspartates in constituting one face of the S1/S1′ subsites (*16*−*18*). While the structural contributions of other S1/S1′ subsite residues can be studied by conventional mutagenesis techniques, the catalytic aspartates, essential for protease activity (*19*, *27*, *28*), cannot be altered to determine if these aspartates have any structural influence on the S1/S1′ subsites. To understand the structural contributions of Asp-125 and Asp-25 to the S1/S1′ subsites, we have

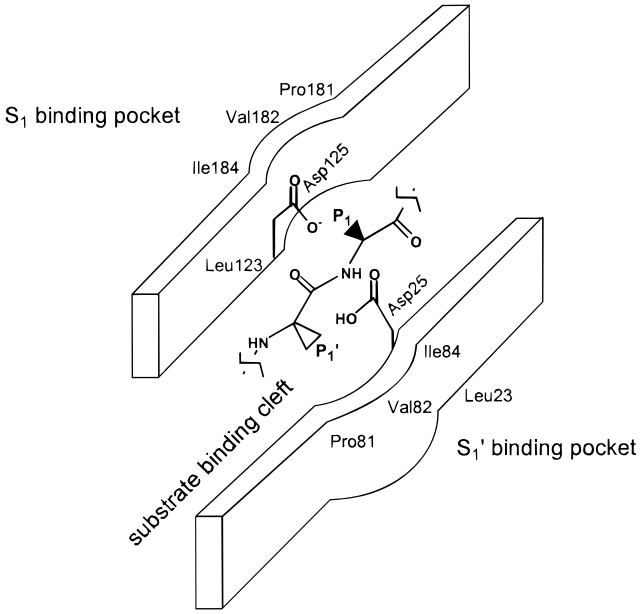

FIGURE 1: Schematic representation of the active site cleft of HIV-1 protease. Two amino acids of the substrate flanking either side of the scissile bond are shown in the center of the diagram. Amino acid residues that line the two substrate binding pockets (S1 and S1′) are proposed to form van der Waals contacts with the amino acid side chains of the substrate (P1 and P1′). By convention, amino acid residues of one monomer are numbered 1−99, while the residues from the other monomer are numbered 101−199. The lytic water molecule, normally coordinated between the catalytic aspartates, has been deleted for clarity.

incorporated a series of modified aspartic acid analogues site specifically within tethered dimers of HIV-1 protease using chemically misacylated suppressor tRNAs during in vitro mRNA translation (*29*−*49*). Because these aspartic acid analogues all maintained the carboxylate functionality necessary for catalysis, the tethered dimers could be assayed to study how subtle structural alterations of the active site aspartates influenced the proteolysis of synthetic protease substrates.

In this study, we report the preparation and analysis of a series of HIV-1 protease-tethered dimers bearing unnatural aspartic acid analogues at either Asp-25 or Asp-125. Several different aspartic acid analogues were studied to extend recent findings concerning the effects of structural alteration of the aminoacyl moiety on the ability of the derived suppressor tRNA to function in the peptidyltransferase reaction at UAG codons. Three of the derivatives were used to prepare HIV-1-tethered dimer analogues that were studied in some detail to define the effects of the substitutions on protease function. Thus, tethered dimers containing *erythro*-β-methylaspartic acid, *threo*-β-methylaspartic acid, and β,β-dimethylaspartic acid were prepared and studied as mediators of the proteolysis of two different HIV-1 protease substrates. To ensure that the altered protease activities were not a consequence of fundamental chemical differences between aspartic acid and the incorporated analogues, pH titration assays and inactivation studies, the latter using the aspartyl protease inhibitor 1,2-epoxy-3-(4-nitrophenoxy)propane, were undertaken. Also carried out were molecular dynamics simulations of the S1′ binding pocket bearing the aspartic acid analogues, to define possible perturbations of the geometry of the pocket resulting from structural alteration of the catalytic aspartates. The accumulated results suggest

that the catalytic residues comprise a structural component of the S1/S1′ subsite and may interact cooperatively with other residues within the subsite, particularly, Val-82/Val-182 and Ile-84/Ile-184.

EXPERIMENTAL PROCEDURES

General Methods and Materials. Amino acid mixtures used during the translation experiments were purchased from Promega Corp. (Madison, WI). T4 RNA ligase and endonuclease *Fok*I were obtained from New England Biolabs (Beverly, MA). Kits for plasmid isolation were purchased from PGC Scientific (Gaithersburg, MD). While isopropyl β-D-thiogalactopyranoside was from Boehringer Mannhiem (Indianapolis, IN), all other biochemicals and enzymes, including NTPs, phosphoenolpyruvate, and pyruvate kinase, were obtained from Sigma Chemicals (St. Louis, MO). T7 RNA polymerase was purchased from Epicentre Technologies (Madison, WI). The HIV-1 protease substrates, anthranilyl-Lys-Ala-Arg-Val-Nle-(*p*-NO_2)-Phe-Glu-Ala-Nle-NH_2, and 4-[4-(dimethylamino)phenylazo]benzoyl-Ser-Gln-Asn-Tyr-Pro-Ile-Val-Gln-5-[(2-aminoethyl)amino]naphthalene-1-sulfonic acid were purchased from Bachem (King of Prussia, PA). Ni-NTA agarose was purchased from Qiagen Inc. (Chatsworth, CA). [^{35}S]Methionine (1000 Ci/mmol, 10 μCi/μL) was from Amersham Corp. Nitroveratryloxycarbonyl (NVOC)-protected pdCpA derivatives of aspartic acid, β,β-dimethylaspartic acid, *threo*-β-methylaspartic acid, and *erythro*-β-methylaspartic acid were prepared as described in ref *50*.

Fluorescence spectral data were obtained using a Hitachi F2000 fluorescence spectrophotometer. Phosphorimager analysis was carried out using a Molecular Dynamics 400E PhosphorImager equipped with ImageQuant version 3.2 software. Radioactivity measurements employed a calibrated phosphorimager screen, permitting correlation of the pixel density of the image directly to the amount of radioactivity present in the sample. Since the six methionines incorporated into HIV-1 protease had a known specific activity, this permitted quantification of the amount of enzyme synthesized, and hence its specific activity.

Construction of Dimeric HIV-1 Protease Expression Plasmids. The tethered dimers of HIV-1 protease, pPRPR and pPRPR125, were constructed as described previously (*49*), using a PCR-mediated technique to link two wild-type genes in tandem with a Gly-Gly linker (*27*). The tethered dimer gene pPR25PR was constructed in a similar fashion except that the N-terminal monomer was derived from a monomeric PR gene bearing the appropriate stop codon (*48*). Because of the toxicity associated with the PRPR gene, a stable *Escherichia coli* cell line necessitated the cloning of PRPR behind a T7 promoter in pET28b(+). In all cases, the gene constructs contained ribosomal binding sites and N-terminal hexahistidine fusion peptides.

Chemical Misacylation of Suppressor tRNA-C_{OH}. Truncated suppressor $tRNA_{CUA}$-C_{OH} used in the chemical misacylation reactions was prepared as described previously (*49*). Chemical misacylation reactions were carried out in 100 μL (total volume) of 50 mM Na Hepes (pH 7.5) containing 0.5 mM ATP, 15 mM $MgCl_2$, 50 μg of suppressor $tRNA_{CUA}$-C_{OH}, 1.0 A_{260} unit of NVOC-protected aminoacyl-pdCpA (5−10-fold molar excess), 20% dimethyl sulfoxide, and 200 units of T4 RNA ligase. The reaction mixture was incubated for 25 min, and then the reaction was quenched by the addition of 0.1 volume of 3 M sodium acetate (pH 4.5). The tRNA was precipitated with 2.5 volumes of ethanol, collected by centrifugation, washed with 70% ethanol, and dried. The product was redissolved in 1 mM KOAc to a final concentration of 1 mg/mL and then irradiated with a 500 W mercury−xenon lamp using Pyrex and water filters. The NVOC-protected aminoacyl-tRNA was cooled in an ice bath during irradiation, which was carried out for 5 min. The deprotected aminoacyl-tRNAs were used in in vitro suppression experiments immediately following deprotection.

S-30 Translation Reactions. In vitro translation reactions were performed in a bacterial S-30 extract containing diminished levels of release factor 1 (*49*). Typically, protease proteins were elaborated in a reaction mixture (100 μL total volume) that contained 10 μg of plasmid DNA in diethyl pyrocarbonate (DEPC)-treated water, 40 μL of premix [35 mM Tris-acetate (pH 7.0), 190 mM potassium glutamate, 2 mM dithiothreitol, 30 mM ammonium acetate, 11 mM magnesium acetate, 20 mM phosphoenolpyruvate, 0.8 mg/mL *E. coli* tRNA, 0.8 mM isopropyl β-D-thiogalactopyranoside, 20 mM GTP and ATP, 5 mM UTP and CTP, and 10 mM cAMP] (*51*), 100 μM amino acids lacking methionine, 50 μM methionine, 40 μCi of [^{35}S]methionine, and 30 μL of S-30 extract that had been heat shocked at 42 °C for 6 min. For pPRPR translation, the in vitro translation reaction mixture included 1200 units of T7 RNA polymerase (200 units/μL). Suppression reaction mixtures (100 μL) contained 25 μg of deprotected misacylated $tRNA_{CUA}$ dissolved in 10 μL of DEPC-treated water, and were maintained at 37 °C for 45 min. Five volumes of acetone was added to precipitate protein from the reaction mixture; the precipitated protein was collected by centrifugation. The protein pellets were dried, and then resuspended in sodium dodecyl sulfate loading buffer prior to polyacrylamide gel electrophoresis (*52*). Dried gels were visualized and analyzed using a Molecular Dynamics phosphorimager followed by exposure to Kodak X-OMAT film.

In Vitro Translation and Dimerization of Wild-Type HIV-1 Protease Monomers. An in vitro S-30 translation reaction was initiated with the plasmid pTHPR (*49*) to express wild-type HIV-1 protease monomer containing a hexahistidine fusion peptide at the amino terminus of the enzyme. The translation reaction mixture (800 μL) containing ^{35}S-labeled protein was precipitated with 2.4 mL of ice-cold acetone, chilled on ice for 15 min, and centrifuged. The supernatant was removed; the pellet was dried, and the residue was redissolved in 20 mM Tris-HCl buffer (pH 7.9) containing 0.5 M NaCl, 5 mM imidazole, 2 mM β-mercaptoethanol, 0.01% (v/v) Triton X-100, 0.25 mg/mL bovine serum albumin (BSA), and 8 M urea. The denatured protein was applied to a 200 μL Ni-NTA agarose column that had been equilibrated with 20 mM Tris-HCl buffer (pH 7.9) containing 0.5 M NaCl, 5 mM imidazole, 2 mM β-mercaptoethanol, 0.01% (v/v) Triton X-100, 0.25 mg/mL BSA, and 8 M urea. The column was washed with 15 column volumes of the equilibration buffer, followed by 6 column volumes of the equilibration buffer containing 20 mM imidazole. The protein was eluted from the column in ten 120 μL aliquots of equilibration buffer containing 1 M imidazole. The amount of ^{35}S-labeled protein in each fraction was determined by

liquid scintillation counting of a portion of each. The fractions containing the purified HIV-1 protease monomers were adjusted with 0.5 M EDTA and 0.5 M dithiothreitol to final concentrations of 5 and 20 mM, respectively. The protein sample was incubated at 37 °C for 45 min to ensure that the protease monomers were reduced prior to refolding. The protein sample was refolded at 4 °C for 16 h by dialysis against 250 volumes of 20 mM Mes buffer (pH 6.0) containing 20 mM dithiothreitol, 0.01% Triton X-100, 5 mM EDTA, and 29% glycerol (v/v). The amount of reconstituted HIV-1 protease was calculated on the basis of [^{35}S]methionine content.

HIV-1 Protease Assay. HIV-1 protease activity in the crude S-30 translation reactions was measured by quantifying the increase in fluorescence following treatment of the substrates anthranilyl-Lys-Ala-Arg-Val-Nle-(*p*-NO_2)-Phe-Glu-Ala-Nle-NH_2 or 4-[4-(dimethylamino)phenylazo]benzoyl-Ser-Gln-Asn-Tyr-Pro-Ile-Val-Gln-5-[(2-aminoethyl)amino]naphthalene-1-sulfonic acid. A typical assay contained 9.1 μM anthranilyl-Lys-Ala-Arg-Val-Nle-(*p*-NO_2)-Phe-Glu-Ala-Nle-NH_2 or 10 μM 4-[4-(dimethylamino)phenylazo]benzoyl-Ser-Gln-Asn-Tyr-Pro-Ile-Val-Gln-5-[(2-aminoethyl)amino]naphthalene-1-sulfonic acid and 4.8 nM crude HIV-1 protease-tethered dimer (40−50 μL of the translation reaction mixture) in 900 μL of 50 mM Mes (pH 6.0) containing 1 mM EDTA, 0.9 M NaCl, 1 mM dithiothreitol, 10% glycerol, 0.1% Triton X-100, and 5% dimethyl sulfoxide. All reaction components were combined, with the exception of the substrate, and incubated at 23 °C for 10 min. The reaction was then initiated by addition of the substrate, and the rate of fluorescence increase was measured [(for anthranilyl-Lys-Ala-Arg-Val-Nle-(*p*-NO_2)-Phe-Glu-Ala-Nle-NH_2, excitation at 337 nm and emission at 420 nm; for 4-[4-(dimethylamino)phenylazo]benzoyl-Ser-Gln-Asn-Tyr-Pro-Ile-Val-Gln-5-[(2-aminoethyl)amino]-naphthalene-1-sulfonic acid, excitation at 340 nm and emission at 490 nm] at 23 °C. Linear initial rate data were obtained from single time points ($t \leq 300$ s).

pH Titration of HIV-1 Protease. The pH dependencies of HIV-1 protease and elaborated analogues were investigated using a published assay, essentially as described previously (*53*). The protease assays used to determine pH titration curves were carried out in 50 mM Mes and 50 mM Tris-HCl buffer system, at varying pHs, containing 50 mM glycine, 50 mM sodium acetate, 1 mM dithiothreitol, 1 mM EDTA, 0.2 M NaCl, 0.1% Triton X-100, 9.1 μM anthranilyl-Lys-Ala-Arg-Val-Nle-(*p*-NO_2)-Phe-Glu-Ala-Nle-NH_2, 2.4 nM crude tethered protease dimer (20−25 μL of the translation reaction mixture), or 2.4 nM purified monomeric HIV-1 protease (900 μL total reaction volume). All reaction components were mixed, except for the substrate, and incubated at 23 °C for 10 min. The reaction was initiated by the addition of the substrate, and the rate of fluorescence increase was monitored at 23 °C (excitation wavelength of 337 nm and emission wavelength of 420 nm). The theoretical curves for the bell-shaped pH−specific activity profiles were calculated by nonlinear regression analysis according to the method of Szeltner and Polgár (*54*).

Molecular Dynamics of HIV-1 Protease. Molecular dynamics simulations were carried out using CHARMM (*55*), part of the computer modeling software package Quanta97 (Molecular Simulations, Inc.). A minimized structure of a tethered dimer of HIV-1 protease was downloaded from the Brookhaven Protein Data Bank (PDB entry 1HVC) (*56*). The inhibitor that was coordinated within the active site cleft of the enzyme was deleted, and any missing protons were constructed using H-Build (*57*). The unnatural aspartic acid side chains at position 25 were constructed using the builder function of Quanta97, and the resulting structures were minimized (50 steepest descent steps) to equilibrate the structure prior to starting 100 ps of full molecular dynamics. All atoms were fixed in space except for the mobile zones of residues 23−28 and 81−86. During the simulation, all bond lengths were constrained using the SHAKE algorithm (*58*). Simulation was performed in three segments. (i) The enzyme was heated from 150 to 300 K for 40 ps. (ii) Equilibration was carried out at 300 K for 10 ps. (iii) Dynamics simulation was performed for 100 ps at 300 K. Data were collected every 1 ps, and the average structures were calculated. The total run time using a Silicon Graphics Crimson workstation was 5 days.

RESULTS

Through the use of tRNAs that have been activated with noncognate amino acids, many peptides and proteins containing amino acid analogues that do not normally occur in nature have been elaborated (*29*−*49*). To produce proteins containing modified amino acids at a single site, a unique codon is employed in combination with a misacylated tRNA bearing a corresponding anticodon. The most widely utilized combination has involved the use of the stop codon, UAG, placed at the intended position of amino acid incorporation, and a chemically misacylated suppressor tRNA capable of reading through that particular nonsense codon. The general strategy is illustrated in Figure 2 and has been employed successfully in our laboratory for the elaboration of a number of different proteins, including HIV-1 protease (*41*, *43*−*49*).

Elaboration of HIV-1 Protease Utilizing Unnatural Aspartic Acid Analogues. To evaluate how the structure of the catalytic aspartic acids might influence the proteolysis of the substrate, a series of unnatural aspartic acid analogues was incorporated within the tethered dimer of HIV-1 protease at position 25 (PR25PR) or 125 (PRPR125). Among the mutant proteases that were produced, several contained aspartic acid analogues having a β-methyl substituent to probe the structural constraints of the S1/S1′ binding pockets of the enzyme. On the basis of the crystal structure of inhibitor-bound complexes of HIV-1 protease, the amino acid residues Val-82/Val-182 as well as Ile-84/Ile-184 are involved in forming the walls of a hydrophobic pocket in which the P1/P1′ side chains interact (*7*−*9*). The active site aspartate residues line another face of the hydrophobic pocket such that P1/P1′ interactions within the S1/S1′ binding pockets may help to orient the aspartates toward the scissile bond of the substrate and promote proteolysis.

Unlike the naturally occurring homodimer of HIV-1 protease, the tethered dimer has been shown to fold readily into an active form that could be assayed directly from an in vitro translation mixture and was preferred in these studies so lengthy purification and dimerization schemes typically required for the homodimer could be avoided (*48*). More importantly, the use of the tethered dimer construct allowed the unnatural amino acids to be substituted one at a time, at either position 25 or 125, so that any change in enzymatic activity could be attributed to that specific substitution.

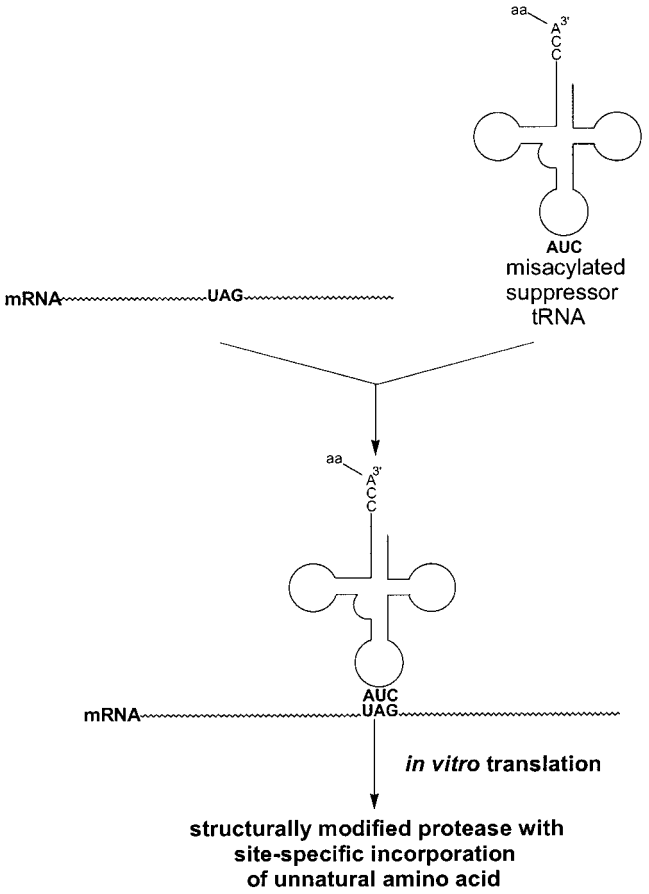

FIGURE 2: Overall strategy employed for the in vitro elaboration of HIV-1 protease containing unnatural aspartic acid derivatives at either position 25 or 125.

The synthesis of a number of analogues of HIV-1 protease modified at single, predetermined sites was effected using the general strategy for the synthesis of proteins containing unnatural amino acids (Figure 2). In this specific case, tethered HIV-1 protease gene constructs containing an amber (UAG) stop codon at position 25 or 125 (Figure 3) were transcribed and translated in a coupled XAC-RF S-30 bacterial extract containing diminished levels of release factor 1 (*49*). Expression of these tethered dimer gene constructs to afford the full-length 23 kDa protein was dependent on the presence of a chemically misacylated suppressor tRNA. Preparation of the misacylated $tRNA_{CUA}$s employed for the readthrough of nonsense codons was accomplished by T4 RNA ligase-mediated coupling of N-protected 2′(3′)-*O*-aminoacyl-pdCpA derivatives to tRNA transcripts lacking the 3′-terminal cytidine and adenosine moieties (*43*, *49*).

Following chemical misacylation with 11 different unnatural derivatives of aspartic acid, the suppressor $tRNA_{CUA}$s were employed for the elaboration of HIV-1 protease-tethered dimers altered at position 25 or 125. In the presence of the misacylated $tRNA_{CUA}$s, several full-length proteases were generated, including analogues containing *erythro*-β-methylaspartic acid, *threo*-β-methylaspartic acid, β,β-dimethylaspartic acid, cysteic acid, *N*-methylaspartate, and *erythro*-carboxyproline (Figures 4 and 5). The ability of a given misacylated $tRNA_{CUA}$ to suppress a nonsense codon at position 25 or 125 was quantified by phosphorimager analysis, and the results are summarized in Table 1. As shown, the incorporation of aspartic acid at positions 25 and 125 proceeded in 9 and 18% yields, respectively, and proved to be comparable in replicate assays. The incorporation of the β-methylaspartic acid analogues proceeded with suppression efficiencies ranging from 11 to 15%, depending upon the structure of the amino acid substituted and the position in the gene at which that substitution was made. Similarly, cysteic acid, *N*-methylaspartic acid, *erythro*-carboxyproline, allylaspartate, β,β-dimethylaspartic acid allyl ester, and methylaspartate were incorporated within the tethered dimers of HIV-1 protease with varying levels of readthrough ranging from 5 to 98%. The aspartic acid analogues α-methylaspartic acid and phosphonoalanine failed to yield full-length mutants above background readthrough levels. The 16 kDa band in Figures 4B and 5B resulted from termination at the UAG codon at position 125, presumably due to active release factor 1 still present in the heat-shocked S-30 extract (*49*). The truncated band for termination at position 25 was too small to be detected by 15% SDS−polyacrylamide gel electrophoresis under the conditions that were employed. Replicate experiments demonstrated relatively little variation from one experiment to another; the intrinsic error due to experimental manipulation was estimated to be ±3%.

While no single factor accurately predicts the extent to which a specific amino acid will be successfully incorporated during in vitro translation, the use of amino acids having charged substituents typically results in lower levels of UAG suppression. As observed in previous reports (*43*, *48*), masking the negative charge of the β-carboxylate moiety of aspartic acid was found to increase the level of UAG codon readthrough in dihydrofolate reductase and monomeric HIV-1 protease. In the case presented here, aspartic acid analogues having either an allyl ester or methyl ester protecting group on the β-carboxylate moiety increased the level of incorporation 5−10-fold in the HIV-1-tethered dimer. This tendency presumably reflects improved interactions with the EF-Tu·GTP complex, which has been observed to bind acylated tRNAs bearing charged residues less efficiently than tRNAs acylated with uncharged amino acids (*59*).

Proteolysis of Synthetic Substrates Mediated by Tethered Dimer Analogues of HIV-1 Protease. The known sequences of HIV-1 PR cleavage sites constitute a diverse collection of potential substrates, and generalizations concerning which peptide sequences might serve as potential HIV-1 PR substrates have also been postulated. One particular classification scheme groups possible substrate sequences into two encompassing families (*60*). In the first family, an aromatic amino acid and proline are characteristically found at P1 and P1′, respectively, while the second maintains hydrophobic residues that flank the scissile bond. To evaluate whether subtle structural changes in the S1/S1′ binding sites led to changes in proteolytic processing of substrate, structurally altered tethered dimers of HIV-1 PR bearing β-methylaspartic acid analogues at position 25 or 125 were assayed for their ability to proteolyze a fluorogenic substrate from each family. The first synthetic substrate (substrate **A**, *o*-aminobenzoyl-K-A-R-V-Nle-NPh-E-A-Nle-NH_2), mimicking a *gag-pol* processing site located at the capsid and nucleocapsid junction, contained norleucine at P1, *p*-nitrophenylalanine at P1′, and a characteristic glutamate at P2′; the second substrate (substrate **B**, DABCYL-S-Q-N-Y-P-I-V-Q-EDANS), representing the cleavage site at the matrix−

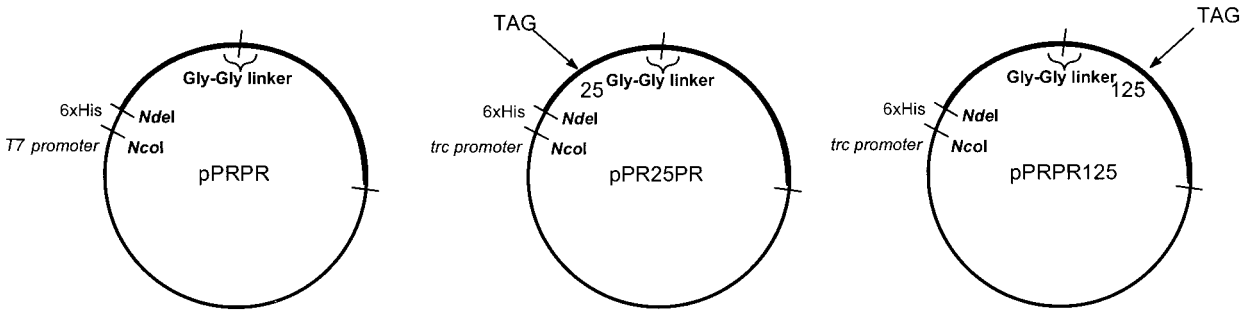

FIGURE 3: Plasmid constructs used in a coupled, release factor 1-depleted S-30 transcription/translation system for the synthesis of the tethered dimer of HIV-1 protease (pPRPR), as well as mutants of the tethered dimer containing amino acid substitutions at position 25 (pPR25PR) or 125 (pPRPR125). The plasmid construct pPRPR was found to be toxic to uninduced bacterial cells during culture, and necessitated the use of a silent T7 promoter to prevent promoter leakage and allow plasmid amplification. The plasmid pTHPR, used for the preparation of the wild type, monomeric HIV-1 protease, contains a *trc* promoter, an N-terminal hexahistidine fusion peptide, and a single copy of the protease gene (PR) followed by an in-frame stop codon (UAA).

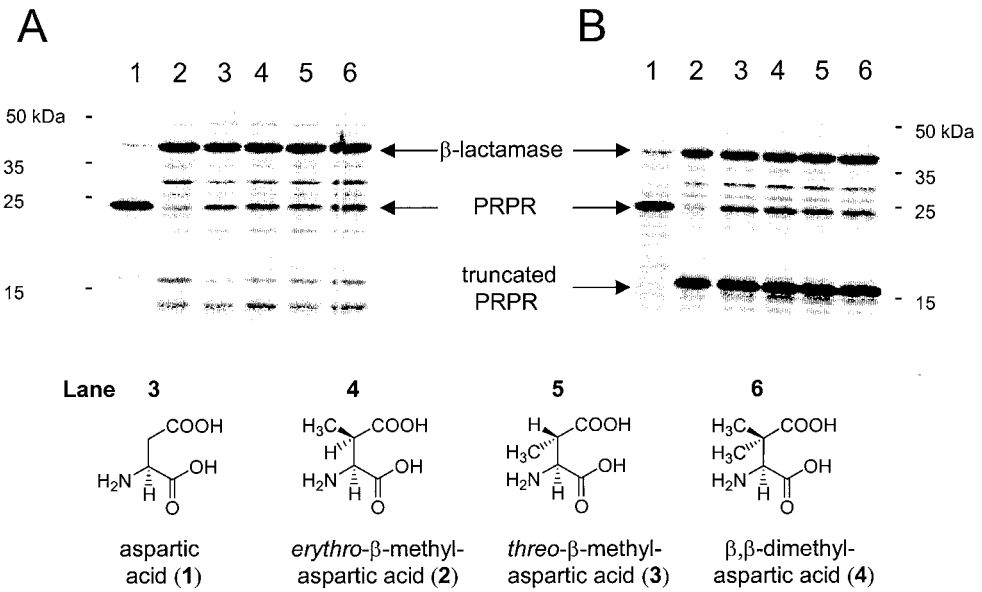

FIGURE 4: Autoradiogram analysis of a 15% SDS−polyacrylamide gel illustrating the in vitro synthesis of the [^{35}S]methionine-labeled tethered dimer of HIV-1 protease analogues modified at either position 25 (A) or 125 (B). Suppression efficiencies are given in Table 1: lane 1, tethered dimer of HIV-1 protease elaborated from wild-type mRNA; lane 2, mRNA from plasmid pPR25PR (A) or plasmid pPRPR125 (B) with full-length unacylated $tRNA^{Phe}_{CUA}$; and lanes 3−6, tethered dimers of HIV-1 protease elaborated from pPR25PR or pPRPR125 in the presence of suppressor $tRNA^{Phe}_{CUA}$ activated with aspartic acid (**1**) (lane 3), *erythro*-*β*-methylaspartic acid (**2**) (lane 4), *threo*-*β*-methylaspartic acid (**3**) (lane 5), and *β*,*β*-dimethylaspartic acid (**4**) (lane 6). The 16 kDa band in panel B resulted from termination at the UAG stop codon at position 125. The structures of the amino acid analogues attached to suppressor $tRNA^{Phe}_{CUA}$ for UAG codon readthrough are shown.

capsid junction, maintained an aromatic amino acid at P1, a proline at P1′, and an asparagine at P2.

Proteolysis of substrate **A** was assayed in the presence of the various *β*-methylaspartate PR25PR analogues to identify which unnatural amino acids, if any, would alter the specific activity of the modified protein relative to that of the wild-type tethered dimer, PRPR. To ensure translational accuracy, the specific activity of PR25PR synthesized from UAG codon readthrough by an aspartylated suppressor $tRNA^{Phe}_{CUA}$ was measured and found to be 4.1×10^5 units min^{-1} mg^{-1}, i.e., 97% of that of PRPR (Table 2). Unexpectedly, the incorporation of *erythro*-*β*-methylaspartic acid reproducibly yielded an HIV-1 protease analogue having a specific activity of 5.5×10^5 units min^{-1} mg^{-1}, i.e., 29% greater than that of PRPR itself. In contrast, incorporation of either *threo*-*β*-methylaspartic or *β*,*β*-dimethylaspartic acid into PR25PR resulted in much lower specific activities. For example, introduction of *threo*-*β*-methylaspartic acid into position 25 provided a PRPR analogue having a specific activity of 0.5 $\times 10^5$ units min^{-1} mg^{-1}, an 87% decrease in specific activity relative to that of PRPR. Moreover, incorporation of *β*,*β*-dimethylaspartic acid yielded a protease analogue having no observable proteolytic activity.

To determine whether the adverse effects of the *threo*-*β*-methylaspartic acid and *β*,*β*-dimethylaspartic acid substitutions within the active site of HIV-1 protease were substrate specific, substrate B was used to measure the catalytic efficiencies of the PR25PR analogues (Table 2). The analogue containing *erythro*-*β*-methylaspartic acid had a specific activity of 4.3×10^4 units min^{-1} mg^{-1}, i.e., only 73% as active as PRPR. Interestingly, increasing the hydrophobic bulk in the S1/S1′ binding pocket with either *threo*-*β*-methylaspartic acid or a *β*,*β*-dimethylaspartic mutant did not affect the specific activity as drastically as in the case of substrate **A**. The *threo*-*β*-methylaspartic acid and *β*,*β*-dimethylaspartic acid analogues of HIV-1 protease had specific activities of 45 and 10%, respectively, of those determined for PRPR. While the individual specific activities

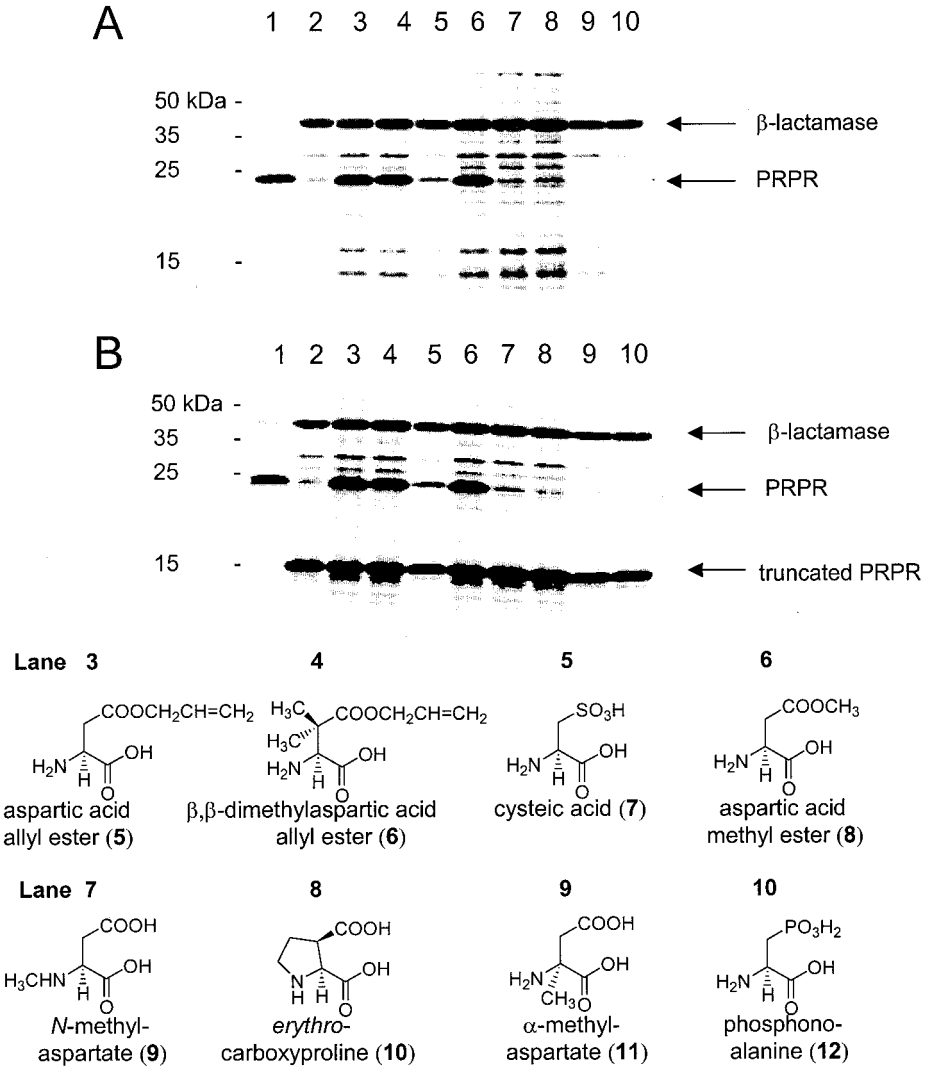

FIGURE 5: Autoradiogram analysis of a 15% SDS−polyacrylamide gel illustrating the in vitro synthesis of HIV-1 protease-tethered dimer analogues. Protein synthesis was carried out in vitro in the presence of [^{35}S]methionine, mRNA containing a UAG codon at position 25 (A) or 125 (B), and an unacylated suppressor tRNA (lane 2) or a misacylated suppressor tRNA (lanes 3−10). Suppression efficiencies are given in Table 1: lane 1, HIV-1 protease dimer elaborated from wild-type mRNA; lane 2, full-length unacylated $tRNA^{Phe}_{CUA}$; lane 3, aspartic acid allyl ester (**5**); lane 4, *β*,*β*-dimethylaspartic acid allyl ester (**6**); lane 5, cysteic acid (**7**); lane 6, aspartic acid methyl ester (**8**); lane 7, *N*-methylaspartate (**9**); lane 8, *erythro*-carboxyproline (**10**); lane 9, α-methylaspartate (**11**); and lane 10, phosphonoalanine (**12**). The structures of the amino acids incorporated into positions 25 and 125 of the dimer of HIV-1 protease are shown.

of the various PR25PR mutants were different, a general trend is readily apparent from the data collected with substrates **A** and **B**. A rank order can be established among the specific activities depending upon the orientation of the *β*-methyl substituent of the incorporated aspartic acid analogue.

Also prepared for study were analogues of HIV-1 protease containing modified aspartates at position 125. Because of the C_2 symmetry of HIV-1 protease, substitution of *β*-methylaspartic acid analogues into position 125 of the tethered dimer should yield proteins having specific activities equivalent to those at position 25 in the presence of an identical substrate. In replicate proteolytic assays with substrate **A**, the incorporation of aspartic acid into PRPR125 led to a protein having a specific activity which was only 78% of that of PRPR. The only difference between the S-30 translation reactions expressing PR25PR and PRPR125 was the presence of a 16 kDa protein resulting from termination at position 125. A previous study by Babé et al. (*61*) demonstrated that the addition of defective protease monomers, lacking critical elements necessary for catalysis, to the catalytically competent wild-type enzyme inhibited substrate proteolysis. Addition of a 4-fold molar excess of defective monomer was found to substantially inhibit proteolytic activity through the exchange of catalytically competent monomers for defective monomers to generate inactive heterodimers (*61*). In the case presented here, even though the constituent monomers in the tethered dimer are physically linked, the dimer presumably maintains an equilibrium between folded and unfolded states. It was thought that the presence of the nonfunctional 16 kDa truncated product during assay may have inhibited substrate proteolysis by binding to the tethered dimer and preventing the full-length enzyme from assuming its native conformation, crucial for maximal activity. When varying ratios of the truncated tethered dimer were mixed with PRPR, substrate processing was inhibited in direct proportion to the amount of truncated dimer that was added. With a 4-fold molar excess of truncated dimer, the proteolytic reaction involving the wild-type tethered dimer and substrate **A** was inhibited by 20%,

Table 1: Synthesis of Structurally Altered HIV-1 Protease-Tethered Dimers from mRNAs Containing a UAG Codon at Position 25 or 125

amino acid[a]	suppression efficiency (%)[b] in XAC-RF S-30[c]	
	position 25	position 125
—[d]	1	2
aspartic acid	9	18
erythro-β-methylaspartic acid	11	14
threo-β-methylaspartic acid	13	12
β,β-dimethylaspartic acid	15	12
cysteic acid	12	10
N-methylaspartic acid	11	9
erythro-carboxyproline	13	5
α-methylaspartic acid	nd[e]	nd[e]
phosphonoalanine	nd[e]	nd[e]
allylaspartate	98	96
β,β-dimethylaspartate allyl ester	95	95
aspartic acid methyl ester	97	96

[a] Introduced as an activated ester of the suppressor tRNA. [b] Relative to the synthesis of HIV-1 protease from wild-type mRNA in the absence of any suppressor tRNA. 5′-Monophosphorylated yeast $tRNA^{Phe}_{CUA}$ was employed for all experiments. [c] Heat shocked for 6 min. [d] Unactivated full-length suppressor tRNA. [e] nd, not detected.

suggesting that the truncated dimer was interacting with PRPR in an unproductive fashion and thereby limiting the maximal rate of catalysis (data not shown). By measuring the amount of inhibition at various molar ratios of truncated dimer to PRPR, we generated a standardized curve and corrected the activity data of PRPR125 analogues.

After data correction, the elaborated PRPR125 analogues still demonstrated some differences in specific activity patterns, relative to those observed for the PR25PR analogues in the presence of substrate **A** (Table 3). As was found for the PR25PR analogues, PRPR125 containing *erythro*-β-methylaspartate again had the greatest specific activity. However, the specific activity of the PRPR125 analogue containing *erythro*-β-methylaspartate was only 58% of that observed for PRPR, compared to the value of 129% noted previously for the same substitution in PR25PR. Differences in specific activity were also observed for PRPR125 analogues containing *threo*-β-methylaspartate and β,β-dimethylaspartate. Contrary to the relative activities associated with the same PR25PR substitutions (Table 2), the analogue containing β,β-dimethylaspartate demonstrated a relative specific activity of 16% while that containing *threo*-β-methylaspartate was inactive. The variation in the specific activities of identical aspartic acid analogue substitutions at positions 25 and 125 must reflect a substrate orientation bias within the active site cleft of the tethered dimer proteases. Presumably, structural perturbations of the active site binding cleft arising from the physical attachment of the two monomeric units in PRPR directly contribute to a lack of symmetry in the protease that is further exacerbated by the presence of an unnatural amino acid. This interpretation was further supported by the measured pH dependence of PRPR and PR, as discussed below.

pH Titration of Modified Tethered Dimers of HIV-1 Protease. The pH dependence of the peptidolytic reaction of PRPR compared to that of recombinant PR was examined previously over a pH range of 3−10.5, and the pH at which the activity of PRPR was maximal was shifted 1 pH unit from 6.5 to 7.5 (*27*). As in the case of other aspartic proteinases, HIV-1 PR exhibits strong H-bonding between Asp-25 and Asp-125 such that the pK_a values of these residues become altered, one being lower and the other higher than that of an ordinary carboxyl group (*62*). DiIanni et al. (*27*) proposed that by physically tethering the monomers of PR with a Gly-Gly linker subtle structural alterations in the four-stranded β-sheet region between the linker region and the floor of the active site cleft may have caused a distortion of the catalytic aspartates and a disruption of H-bonding, thereby resulting in a shift of the pH optimum. To investigate whether the β-methylaspartic acid substituted tethered dimers exhibited similar phenomena, the specific activities of the PRPR analogues were measured as a function of pH.

Initially, the pH optima for PRPR prepared in vitro and purified recombinant PR were determined in the presence of substrate **A**. While the monomeric protease exhibited maximal activity at pH 5.0, the profile for the wild-type PRPR was shifted 1 pH unit to 6.0 (Figure 6). Although assayed under different buffer conditions, the 1 pH unit shift for PRPR is identical to the observations of DiIanni et al. (*27*). Moreover, the pH−specific activity profile maintains a bell shape, suggesting that the ionization of Asp-25 and Asp-125 occurs as it does in the case of PR (*53*) and consistent with the interpretation that the general acid−general base mechanism typically associated with PR is also the catalytic mechanism utilized by PRPR.

The analogues of the tethered dimer of HIV-1 protease were studied not only to examine the chemical behavior of the active site aspartates at various pH values but also to yield insight into the extent of interaction between these residues as a predictor of structural alteration within the S1/S1′ binding pocket. Relative to PRPR, the PR25PR analogue containing *erythro*-β-methylaspartate was found to have a pH−rate profile that was shifted 0.5 pH unit to a new pH optimum of 6.5 (Figure 7). The pH−rate profile for the mutant PR25PR containing *threo*-β-methylaspartate was shifted 1.0 pH unit further, exhibiting maximal activity at pH 7.0. Because the PR25PR analogue substituted with β,β-dimethylaspartate did not exhibit any proteolytic activity in previous assays (Table 2), the PRPR125 analogue containing β,β-dimethylaspartate, which exhibited limited activity (Table 3), was used in the pH titration assay. As shown in Figure 7, there was a pH shift (0.7 pH unit) in the pH−specific activity profile for this analogue, which exhibited a maximal rate of proteolysis at pH 6.7. Although this pH shift was not as great as in the case of *threo*-β-methylaspartic acid, both mutants demonstrated narrow, effective pH ranges in which the proteases proved to be active. Plausibly, these narrow pH profiles may arise from further structural perturbation in the active site, thus altering the H-bonding interactions between the modified and unmodified catalytic residues.

It could be argued that the increases in pH optima observed for the protease analogues were due to changes in the pK_as of the side chain carboxylates occasioned by introduction of methyl groups at the β-position. However, if this were true, it would be anticipated that the pH optima for the protease analogues containing *erythro*- and *threo*-β-methylaspartates would be identical due to their chemical equivalence, and that the pH optimum of the analogue containing β,β-dimethylaspartate would be shifted to the highest pH

Table 2: Proteolytic Activities of PR25PR Analogues As Compared to PRPR in the Presence of Two Synthetic Substrates

	substrate **A**		substrate **B**	
enzyme	Abz[a]-K-A-R-V-Nle↓NPh-E-A-Nle-NH_2 specific activity ($\times 10^5$ FU min^{-1} mg^{-1})[c]	% wild-type activity	DABCYL-EDANS substrate[b] specific activity ($\times 10^4$ FU min^{-1} mg^{-1})[c]	% wild-type activity
PRPR	4.3 ± 0.3	100	6.0 ± 0.3	100
PR25PR aspartic acid	4.1 ± 0.3	97	5.5 ± 0.1	92
erythro-β-methylaspartic acid	5.5 ± 0.3	129	4.3 ± 0.3	73
threo-β-methylaspartic acid	0.5 ± 0.1	13	2.7 ± 0.6	45
β,β-dimethylaspartic acid	nd[d]	0	0.6 ± 0.1	10

[a] Abz, *o*-aminobenzoyl. [b] The sequence of the substrate is 4-[4-(dimethylamino)phenylazo]benzoyl (DABCYL)-S-Q-N-Y↓P-I-V-Q-5-[(2-aminoethyl)amino]naphthalene-1-sulfonic acid (EDANS). [c] The specific activity was determined by the rate of increase in fluorescence intensity units (FU) per minute per milligram of protease. [d] nd, no detectable protease activity above background levels.

Table 3: Proteolytic Activities of PRPR125 Analogues As Compared to That of PRPR

	substrate **A**	
PRPR125	Abz[a]-K-A-R-V-Nle↓NPh-E-A-Nle-NH_2 specific activity ($\times 10^5$ FU min^{-1} mg^{-1})[b]	% wild-type activity[c]
aspartic acid	4.3 ± 0.5	100
erythro-β-methylaspartic acid	2.5 ± 0.4	58
threo-β-methylaspartic acid	nd[d]	0
β,β-dimethylaspartic acid	0.7 ± 0.1	16

[a] Abz, *o*-aminobenzoyl. [b] The specific activity was determined by the rate of increase in fluorescence intensity units (FU) per minute per milligram of protease. [c] The specific activity was corrected for protease inhibition by the 16 kDa truncated dimer. [d] nd, no detectable protease activity above background levels.

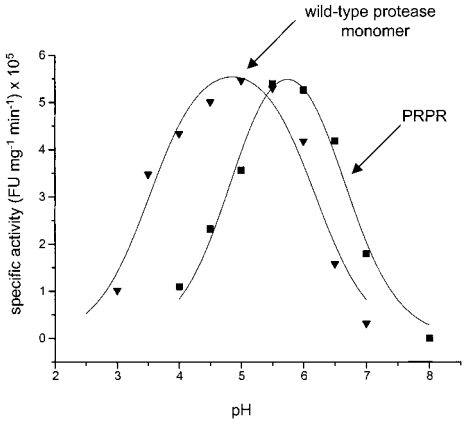

FIGURE 6: Specific activities of monomeric and dimeric forms of HIV-1 protease vs pH. The monomer (▼) and tethered dimer (■) of HIV-1 protease (2.4 nM) were incubated with the anthranilyl-K-A-R-V-Nle↓NPh-E-A-Nle-NH_2 substrate at the specified pH, while the extent of substrate cleavage was determined by an increase in fluorescence. The specific activity is given as the rate of increase in fluorescence intensity units (FU) per minute per milligram of protease.

value. However, as demonstrated in Figure 7, the actual data are inconsistent with this interpretation.

Irreversible Inhibition of Modified Tethered Dimers of HIV-1 Protease. Alteration of the pH profiles of the tethered dimer analogues is most likely due to structural changes in the active site leading to a repositioning of one catalytic residue with respect to the other. However, by introduction of methyl groups on the β-carbon of the side chain of aspartic acid, the pK_a of the residue may have been slightly altered. Even though the majority of tethered dimer analogues

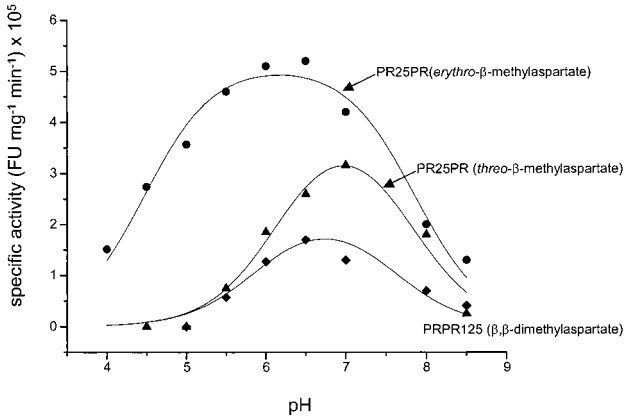

FIGURE 7: Specific activities of tethered dimer analogues of HIV-1 protease, containing *erythro*-β-methylaspartic acid (●) or *threo*-β-methylaspartic acid (▲) at position 25 and β,β-dimethylaspartic acid (◆) at position 125, vs pH. The dimers of HIV-1 protease (2.4 nM) were incubated with the anthranilyl-K-A-R-V-Nle↓NPh-E-A-Nle-NH_2 substrate at the specified pH, while the cleavage reaction was monitored by an increase in fluorescence. The specific activity is given as the rate of increase in fluorescence intensity units (FU) per minute per milligram of protease.

exhibited proteolytic activity, as well as bell-shaped pH titration curves typically associated with aspartyl proteases, the protease analogues were assayed in the presence of a suicide inhibitor to ensure that a small increase in the pK_a of one catalytic residue did not alter the mechanism of inactivation.

Accordingly, a known irreversible inhibitor of aspartyl proteinases was used to probe the active site aspartates for differences between PR25PR analogues and PRPR itself. EPNP, 1,2-epoxy-3-(4-nitrophenoxy)propane, has been demonstrated by protein sequencing and X-ray crystallographic analysis to esterify the active site aspartate residues of pepsin (*63*), as well as HIV-1 protease (*64*). PRPR and PR25PR analogues were pretreated with 10 mM EPNP and assayed for their ability to cleave the synthetic substrate Ac-R-A-S-Q-N-Y-P-V-V-NH_2, similar to the *gag* sequence found at the matrix−capsid junction. After incubation, the extent of protease-mediated cleavage was assessed by HPLC. Wild-type PRPR was observed to proteolyze 87% of the substrate (Table 1 in the Supporting Information). However, after pretreatment with EPNP, only 2% of the substrate was processed. In a similar fashion, PR25PR substituted with *erythro*-β-methylaspartate and *threo*-β-methylaspartate consumed 4.9 and 2.5% of the substrate, respectively, and both were inactivated completely in the presence of EPNP. PR25PR substituted with β,β-dimethylaspartic acid failed to

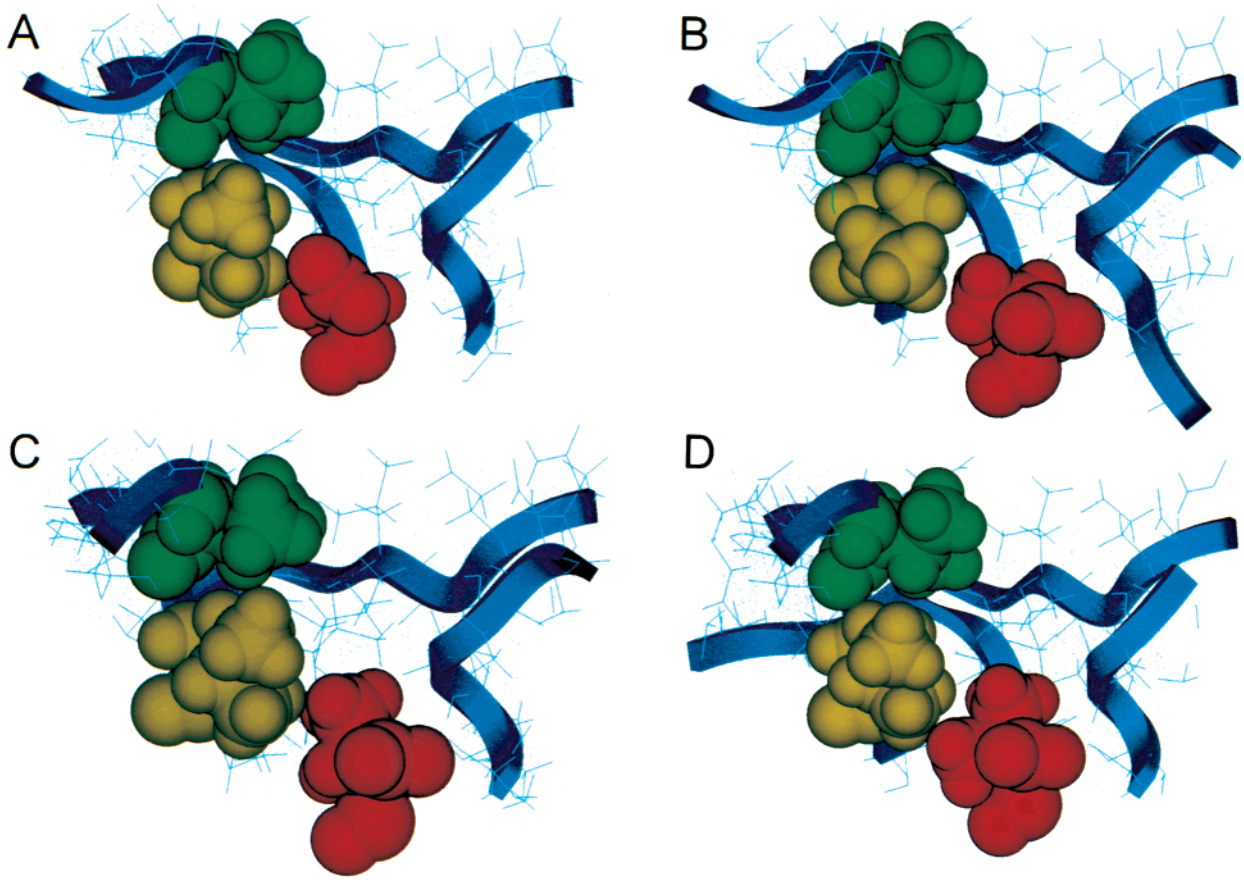

FIGURE 8: Molecular models of the S1′ binding pocket of HIV-1 protease based upon molecular dynamics simulations of a tethered dimer bearing aspartic acid (A), *erythro*-β-methylaspartic acid (B), *threo*-β-methylaspartic acid (C), or β,β-dimethylaspartic acid (D). In each model, residues Val-82 (green), Ile-84 (gold), and position 25 (red) are highlighted for reference.

process the substrate. Although the mutants were active to varying extents, these findings demonstrate the similar susceptibilities to inactivation shared by the elaborated PR25PR mutants and PRPR. These results are thus consistent with the interpretation that any differences between the specific activities of PR25PR analogues and PRPR are a consequence of structural changes within the active site cleft rather than an alteration of the catalytic mechanism due to pK_a shifts of the active site aspartic acid residues.

Molecular Dynamics Simulation of the S1′ Binding Pocket of Modified Tethered Dimers of HIV-1 Protease. To better understand the factors that influence the relative specific activities of the elaborated proteases, the structures of the mutated S1′ binding pockets were modeled using a molecular dynamics simulation (Figure 8). A minimized structure of a related tethered dimer of HIV-1 protease (*56*) was obtained from the Brookhaven Protein Data Bank and served as the initial reference structure from which a series of protease analogues was constructed. The reference structure was altered such that the β-carbon of the β-carboxylate was substituted with either an *erythro*-β-methyl, a *threo*-β-methyl, or a β,β-dimethyl moiety at position 25. The global energy component of all models was minimized, and all atoms were fixed in space except for those residues located around the S1′ binding pocket.

On the basis of a 100 ps molecular dynamics simulation, averaged structures generated models that maintained varying degrees of reorganization of the S1′ binding pocket depending upon the substituted unnatural aspartic acid derivative. The model containing aspartic acid was found to be homologous with the reference structure after dynamics simulation, suggesting that the algorithm used during simulation did not perturb the structure unproductively (Figure 8A). Although similar to the wild-type model, the model depicting the *erythro*-β-methylaspartate demonstrated an S1′ binding pocket that was 0.2 Å wider (8.0 Å) than that for aspartic acid (7.8 Å) (Figure 8B). Two related factors appear to be responsible for the widening the S1′ pocket. First, a rotation of the *erythro*-β-methylaspartate toward the center of the active site cleft occurred to minimize steric occlusion between the *erythro*-β-methyl moiety and the β-methyl moiety of Ile-84. Second, in an attempt to reduce unfavorable steric interactions while at the same time promoting favorable hydrophobic−hydrophobic interactions with *erythro*-β-methylaspartate, the side chain of Ile-84 rotated about its $\alpha-\beta$ carbon−carbon bond. This rotation not only helped relieve unfavorable steric interactions but also helped maintain the geometric integrity of the S1′ binding pocket. As demonstrated in Figure 9, the boundaries of the S1′ binding pocket consist of residues Val-82, Ile-84, and Asp-25 positioned in an angular arrangement. In the case of aspartic acid, the lengths of the two walls between Val-82/Ile-84 and Ile-84/Asp-25 are 4.7 and 7.7 Å, respectively (Figure 9A). Upon S1′ pocket reorganization in the presence of *erythro*-β-methylaspartate at position 25, the relative lengths of the S1′ binding pocket walls are reversed, 7.0 Å between Val-82 and Ile-84 and 4.1 Å between Ile-84 and position 25. While individual lengths of the walls that comprise the

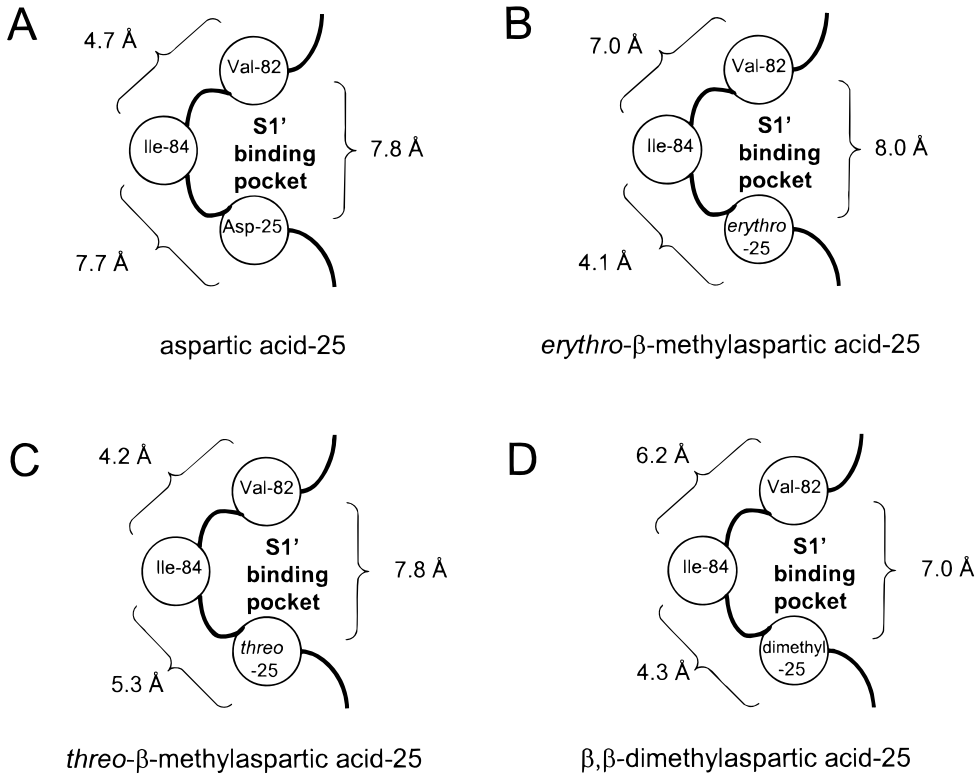

FIGURE 9: Schematic representation of the S1′ binding pocket of HIV-1 protease showing the relative intermolecular distances between Val-82, Ile-84, and position 25 substituted with either aspartic acid (A), *erythro*-*β*-methylaspartic acid (B), *threo*-*β*-methylaspartic acid (C), or *β*,*β*-dimethylaspartic acid (D).

mutated S1′ binding pocket have changed, the overall geometry and depth of the S1′ binding pocket remain similar to those of the wild-type model.

In the models depicting the *threo*-*β*-methyl and *β*,*β*-dimethyl substitutions, Ile-84 was found to remain in a similar position as in the wild-type model. Steric occlusion between the *β*-methyl group of Ile-84 and the *threo*-*β*-methyl moiety in both instances was not observed to occur. Interestingly, the *β*-methyl group of Ile-84 favorably interacted with the *threo*-*β*-methyl moiety via hydrophobic−hydrophobic interactions and did not necessitate Ile-84 repositioning (Figure 8C). Likewise, in the case the *β*,*β*-dimethylaspartate, the *β*-methyl group of Ile-84 hydrophobically packed between the dimethyl groups without Ile-84 being repositioned (Figure 8D). As a consequence of favorable van der Waals interactions within the S1′ binding pocket of both *threo*-*β*-methylaspartate and *β*,*β*-dimethylaspartate mutants, the binding pocket became narrower and shallower as the pocket became more sterically crowded. For the *threo*-*β*-methyl substitution, the width of the S1′ binding pocket remained unchanged (7.8 Å) yet the pocket became shallower by 2.4 Å due to tighter packing between all three residues constituting the S1′ pocket (Figure 9C). As in the case of the *erythro*-*β*-methylaspartate model, the lengths of the walls of the S1′ binding pocket in the *β*,*β*-dimethylaspartate model were reversed compared to the wild-type model; however, unlike that of the *erythro*-*β*-methyl model, the overall geometry was not preserved. While the *threo*-*β*-methylaspartate maintained the shallowest S1′ binding pocket, the entry into the S1′ binding pocket of the *β*,*β*-dimethylaspartate model was the narrowest. The S1′ pocket in the *β*,*β*-dimethylaspartate model was 0.8 Å narrower and 1.5 Å shallower (Figure 9D). These molecular models indicate that very small structural perturbations of the catalytic residues may have profound effects on the overall structure of the S1′ binding pocket, and thus influence the manner in which substrates are bound within the active site and processed.

DISCUSSION

While X-ray crystallographic studies have provided static structures of HIV-1 protease that depict a relatively close spatial proximity between the S1/S1′ binding pockets and the catalytic aspartates (*7*−*9*), no biochemical evidence has been offered previously that demonstrates the involvement of the catalytic aspartates in the formation of the S1/S1′ binding pocket. On the basis of previous X-ray crystal structures of protease−inhibitor complexes (*16*−*18*), we reasoned that the catalytic aspartates may help constitute one face of the S1/S1′ binding pocket and, upon the binding of authentic substrate, be reoriented closer to the scissile bond. Because conventional mutagenesis techniques involving the substitution of natural amino acid residues other than aspartic acid into positions 25 and 125 have simply led to a loss of activity (*19*, *27*, *28*), a number of aspartic acid analogues were incorporated in the active site of the protease (Table 1) using misacylated suppressor tRNAs (*29*−*50*). Three particularly useful derivatives were incorporated with suppression efficiencies that were sufficient to allow the characterization of proteolytic activity of the derived proteases, namely, *erythro*-*β*-methylaspartic acid, *threo*-*β*-methylaspartic acid, and *β*,*β*-dimethylaspartic acid.

The facility with which tethered dimer protease analogues were able to process two HIV-1 protease substrates was dependent upon the orientation of the *β*-methyl group

substituted on the side chain of the aspartic acid analogue. As shown in Table 2, a PR25PR containing *erythro*-β-methylaspartate actually exhibited a 29% increase in specific activity, while the introduction of *threo*-β-methylaspartate resulted in an 87% decrease in activity, and β,β-dimethylaspartate caused a complete loss of activity. While the methyl groups in *erythro*-β-methylaspartic acid and *threo*-β-methylaspartic acid both increase the propensity for unproductive steric interactions within the active site, models based on a 100 ps molecular dynamics simulation (Figure 8B) suggest that in the case of *erythro*-β-methylaspartate a reorganization of the S1/S1′ binding pocket occurs. An unfavorable steric interaction between the β-methyl of *erythro*-β-methylaspartate and the β-methyl of Ile-84 led to a reorganization of the S1/S1′ subsite involving a rotation of the side chain of Ile-84 about its $\alpha-\beta$ carbon−carbon bond as well as a displacement of the catalytic aspartate toward the center of the active site cleft. While the lengths of the walls of the S1/S1′ binding pocket were reversed from those in the wild-type subsite, changing the shape of the pocket slightly (Figure 9), the overall geometry of the binding pocket was well-preserved with a slight widening of the mouth and shallowing of the pocket. This altered subsite geometry helps to explain the increase in specific activity of this mutant when it is assayed in the presence of substrate **A**. In this particular altered subsite conformation, the binding pocket becomes more accessible to a substrate with large hydrophobic residues at P1 and P1′ as found in the case of substrate **A**. Further, with the altered catalytic residue displaced toward the center of the active site cleft, closer to the scissile bond, a more accessible S1/S1′ binding pocket combined with a repositioned catalytic aspartate may function cooperatively to improve substrate recognition and processivity.

Protease analogues containing either *threo*-β-methylaspartic acid or β,β-dimethylaspartic acid exhibited large decreases in specific activity. Models based on molecular dynamics simulations demonstrated that the methyl group unique to *threo*-β-methylaspartate did not interact sterically with the β-methyl of Ile-84 (Figure 8C) and failed to reorganize the geometry of the pocket. Consequently, the *threo*-β-methyl moiety that was directed toward the S1/S1′ binding pocket occluded the pocket in both the *threo*-β-methylaspartate and the β,β-dimethylaspartate protease analogues and led to a corresponding decrease in the specific activity of the enzymes, presumably due to unfavorable substrate binding (Tables 2 and 3). While the catalytic aspartates were predicted by the models to be rotated to the center of the active site cleft as observed for *erythro*-β-methylasparate, the geometry of the S1/S1′ binding pocket became shallower due to the *threo*-β-methyl group blocking P1/P1′ residue entry into the subsite. Additionally, in the case of the β,β-dimethylaspartate substitution, the Ile-84 rotated slightly to orient its β-methyl moiety between the β,β-dimethyl group to effectively stabilize a narrow S1/S1′ binding pocket conformation by van der Waals interactions. As anticipated on the basis of the molecular model, PR25PR substituted with β,β-dimethylaspartic acid when assayed against substrate **A** failed to exhibit proteolytic activity.

Substrate **B**, which contains an aromatic residue and proline at P1 and P1′, respectively, was processed with somewhat different relative efficiencies by the protease analogues. While the PR25PR analogue containing *erythro*-β-methylaspartate was still the most efficient of the analogues in processing substrate **B**, activity was nonetheless reduced relative to that of PRPR (Table 2). Differences in the ability of this analogue to process the two substrates presumably arise from the manner in which the two different classes of substrates are recognized in the S1/S1′ binding subsite. Substrate specificities of HIV-1 protease have been shown to arise from multiple interactions between the side chains of the substrate and the binding subsites within the enzyme (*65*). Because of the extensive recognition between HIV-1 protease and at least six amino acids in a typical substrate, the enzyme exhibits large degrees of adaptability in recognizing and processing varying substrate sequences. Hydrophobic interactions between the P1/P1′ and S1/S1′ binding pocket, as in the case of substrate **A**, tend to greatly influence substrate specificity compared to other amino acid side chains of the substrate (*66*). However, for the substrate class that maintains an aromatic residue and proline at P1 and P1′, as in the case of substrate B, the most prominent factors that determine substrate specificity and processivity involve recognition of P2 and P2′ (*66*). The data in Table 2 support this assertion and demonstrate that replacement of the catalytic aspartates with β-methylaspartate analogues generally alters the proteolysis of substrate **A** to a greater extent than that of substrate **B**, which was especially evident when PR25PR contained *threo*-β-methylaspartate. This phenomenon presumably reflects a significant alteration of the S1/S1′ subsite geometry to preferentially disfavor those substrates that are bound primarily by hydrophobic interactions at P1 and P1′. While the overall "shape and fit" are paramount to the successful binding of the substrate within the active site cleft of HIV-1 protease, these observations emphasize the subtle differences in the manner in which HIV-1 protease binds these two classes of substrates and suggests important structural considerations when designing substrate-based inhibitors.

The accumulated data argue that the catalytic aspartates are an integral part of the S1/S1′ binding pocket, important both catalytically and structurally to substrate processivity. It is interesting to consider these results in the context of cooperative interaction between the residues in the S1/S1′ binding pocket and the catalytic aspartic acid. As demonstrated here, unnatural aspartic acid analogues incorporating relatively small structural changes can dramatically alter substrate processing due to their spatial proximity to the S1/S1′ binding subsites. Moreover, models based on molecular dynamics simulations have implicated the catalytic residues as a structural boundary of these subsites. On the basis of the structural effects apparently imposed on Ile-84 and Val-82 in the S1/S1′ subsite by the modified catalytic aspartates, it seems plausible that in wild-type HIV-1 protease these residues may in turn cooperatively influence the relative orientations of the catalytic residues themselves. On the basis of the observation that Val-82 and Ile-84 tend to be the most prominent viral mutations that lead to HIV resistance against substrate-based inhibitors (*23*−*26*), these residues are implicated in defining the geometry of the S1/S1′ subsite crucial to both inhibitor and substrate recognition. If Val-82 and Ile-84 define the contour of the S1/S1′ subsite and interact hydrophobically with P1 and P1′ of the substrate, it is reasonable to conclude that changes in the relative orientations of Val-82 and Ile-84 induced upon substrate binding

may cooperatively affect the relative orientations of the catalytic aspartates. Due to the observed interactions between the catalytic aspartates and the residues of the S1/S1′ subsite, we suggest that upon substrate binding the S1/S1′ subsites may become slightly distorted to cooperatively direct the β-carboxylates of the catalytic residues toward the scissile bond to help initiate catalysis.

In summary, we have studied HIV-1 protease analogues containing structurally modified catalytic aspartates. Relatively small structural changes in these aspartate residues substantially alter the catalytic competence of the enzyme due to a proposed alteration of the S1/S1′ substrate binding subsites. These results suggest that the catalytic aspartates may not only provide the chemical basis for enzyme catalysis but also provide a structural component that is important during binding of the substrate. Further, interactions with the S1/S1′ subsites may reposition the catalytic aspartates upon substrate binding to help orient the residues closer to the scissile bond.

ACKNOWLEDGMENT

We thank Dr. Mark Van Cleve for assistance in the initiation of this study and Dr. Thomas Meek (SmithKline Beecham Pharmaceuticals) for helpful discussions during the course of this work.

SUPPORTING INFORMATION AVAILABLE

A table describing the effects of EPNP on the function of wild-type HIV-1 protease and three analogues, as well as a description of the Experimental Procedures employed in these experiments. This material is available free of charge via the Internet at http://pubs.acs.org.

REFERENCES

1. Wain-Hobson, S., Sonigo, P., Danos, O., Cole, S., and Alizon, M. (1985) *Cell 40*, 9−16.
2. Kohl, N. E., Emini, E. A., Schleif, W. A., Davis, L. J., Heimbach, J. C., Dixon, R. A. F., Scolnick, E. M., and Sigal, I. S. (1988) *Proc. Natl. Acad. Sci. U.S.A. 85*, 4686−4690.
3. Vogt, V. M. (1996) *Curr. Top. Microbiol. Immunol. 214*, 95−131.
4. Erickson-Viitenan, S., Manfredi, J., Viitanen, P., Tribe, D. E., Tritch, R., Hutchison, C. A., III, Loeb, D. D., and Swanstrom, R. (1989) *AIDS Res. Hum. Retroviruses 5*, 577−591.
5. Vacca, J. P. (1997) *Drug Discovery Today 7*, 261−272.
6. Meek, T. D., Dayton, B. D., Metcalf, B. W., Dreyer, G. B., Strickler, J. E., Gorniak, J. G., Rosenberg, M., Moore, M. L., Magaard, V. W., and Debouck, C. (1989) *Proc. Natl. Acad. Sci. U.S.A. 86*, 1841−1845.
7. Navia, M. A., Fitzgerald, P. M. D., McKeever, B. M., Leu, C.-T., Heimbach, J. C., Herber, W. K., Sigal, I. S., Darke, P. L., and Springer, J. P. (1989) *Nature 337*, 615−620.
8. Wlodawer, A., Miller, M., Jaskólski, M., Sathyanarayana, B. K., Baldwin, E., Weber, I. T., Selk, L. M., Clawson, L., Schneider, J., and Kent, S. B. H. (1989) *Science 245*, 616−621.
9. Lapatto, R., Blundell, T., Hemmings, A., Overington, J., Wilderspin, A., Wood, S., Merson, J. R., Whittle, P. J., Danley, D. E., Geoghegan, K. F., Hawrylik, S. J., Lee, S. E., Scheld, K. G., and Hobart, P. M. (1989) *Nature 342*, 299−302.
10. Darke, P. L., Nutt, R. F., Brady, S. F., Garsy, V. M., Ciccarone, T. M., Leu, C.-T., Lumma, P. K., Freidinger, R. M., Veber, D. F., and Sigal, I. S. (1988) *Biochem. Biophys. Res. Commun. 156*, 297−303.
11. Kotler, M., Katz, R. A., Danho, W., Leis, J., and Skalka, A. M. (1988) *Proc. Natl. Acad. Sci. U.S.A. 85*, 4185−4189.
12. Moore, M. L., Bryan, W. M., Fakhoury, S. A., Magaard, V. W., Huffman, W. F., Dayton, B. D., Meek, T. D., Hyland, L., Dreyer, G. B., Metcalf, B. W., Strickler, J. E., Gorniak, J. G., and Debouck, C. (1989) *Biochem. Biophys. Res. Commun. 159*, 420−425.
13. Toth, M. V., and Marshall, G. R. (1990) *Int. J. Pept. Protein Res. 36*, 544−550.
14. Toser, J., Gustchina, A., Weber, I. T., Blaha, I., Wondrak, E. M., and Oroszlan, S. (1991) *FEBS Lett. 279*, 356−360.
15. Richards, A. D., Phylip, L. H., Farmerie, W. G., Scarborough, P. E., Alvarez, A., Dunn, B. M., Hirel, P.-H., Konvalinka, J., Strop, P., Pavlickova, L., Kostka, V., and Kay, J. (1990) *J. Biol. Chem. 265*, 7733−7736.
16. Wlodawer, A., and Erickson, J. W. (1993) *Annu. Rev. Biochem. 62*, 543−585.
17. Miller, M., Schneider, J., Sathyanarayana, B. K., Toth, M. V., Marshall, G. R., Clawson, L., Selk, L., Kent, S. B. H., and Wlodawer, A. (1989) *Science 246*, 1149−1152.
18. Swain, A. L., Miller, M. M., Green, J., Rich, D. H., Schneider, J., Kent, S. B. H., and Wlodawer, A. (1990) *Proc. Natl. Acad. Sci. U.S.A. 87*, 8805−8809.
19. Loeb, D. D., Swanstrom, R., Everitt, L., Manchester, M., Stamper, S. E., and Hutchison, C. A., III (1989) *Nature 340*, 397−400.
20. Hyland, L. J., Tomaszek, T. A., Jr., Roberts, G. D., Carr, S. A., Magard, V. W., Bryan, H. L., Fahoury, S. A., Moore, M. L., Minnich, M. D., Culp, J. S., DesJarlais, R. L., and Meek, T. D. (1991) *Biochemistry 30*, 8441−8453.
21. Pettit, S. C., Michael, S. F., and Swanstrom, R. (1993) *Perspect. Drug Discovery Des. 1*, 69−83.
22. Bardi, J. S., Luque, I., and Freire, E. (1997) *Biochemistry 36*, 6588−6596.
23. Condra, J. H., Schleif, W. A., Blahy, O. M., Gabryelski, L. J., Graham, D. J., Quintero, J. C., Rhodes, A., Robbins, H. L., Roth, E., Shivaprakash, M., Titus, D., Yang, T., Teppler, H., Squires, K. E., Deutsch, P. J., and Emini, E. A. (1995) *Nature 374*, 569−571.
24. Kaplan, A. H. (1996) *AIDS Res. Hum. Retroviruses 12*, 849−853.
25. Lin, Y., Lin, X., Hong, L., Foundling, S., Heinrikson, R. L., Thaisrivongs, S., Leelamanit, W., Raterman, D., Shah, M., Dunn, B. M., and Tang, J. (1995) *Biochemistry 34*, 1143−1152.
26. Kervinen, J., Thanki, N., Zdanov, A., Tino, J., Barrish, J., Lin, P. F., Colonno, R., Riccardi, K., Samanta, H., and Wlodawer A. (1996) *Protein Pept. Lett. 3*, 399−406.
27. DiIanni, C. L., Davis, L. J., Holloway, M. K., Herber, W. K., Darke, P. L., Kohl, N. E., and Dixon, R. A. F. (1990) *J. Biol. Chem. 265*, 17348−17354.
28. DiIanni, C. L., Darke, P. L., Dixon, R. A. F., and Sigal, I. S. (1990) *Current Research in Protein Chemistry: Techniques, Structure, and Function*, pp 521−528, Academic Press, Orlando, FL.
29. Hecht, S. M., Alford, B. L., Kuroda, Y., and Kitano, S. (1978) *J. Biol. Chem. 253*, 4517−4520.
30. Roesser, J. R., Xu, C., Payne, R. C., Surratt, C. K., and Hecht, S. M. (1989) *Biochemistry 28*, 5185−5189.
31. Noren, C. J., Anthony-Cahill, S. J., Griffith, M. C., and Schultz, P. G. (1989) *Science 244*, 182−188.
32. Robertson, S. A., Noren, C. J., Anthony-Cahill, S. J., Griffith, M. C., and Schultz, P. G. (1989) *Nucleic Acids Res. 17*, 9649−9660.
33. Robertson, S. A., Ellman, J. A., and Schultz, P. G. (1991) *J. Am. Chem. Soc. 113*, 2722−2729.
34. Bain, J. D., Diala, E. S., Glabe, C. G., Wacker, D. S., Lyttle, M. H., Dix, T. A., and Chamberlin, A. R. (1991) *Biochemistry 30*, 5411−5421.
35. Ellman, J. A., Mendel, D., and Schultz, P. G. (1992) *Science 255*, 197−200.
36. Mendel, D., Ellman, J. A., Chang, Z., Veenstra, D. L., Kollman, P. A., and Schultz, P. G. (1992) *Science 256*, 1798−1802.
37. Judice, J. K., Gamble, T. R., Murphy, E. C., de Vos, A. M., and Schultz, P. G. (1993) *Science 261*, 1578−1581.

38. Chung, H.-H., Benson, D. R., and Schultz, P. G. (1993) *Science 259*, 806−809.
39. Cornish, V. W., Benson, D. R., Altenbach, C. A., Hideg, K., Hubbell, W. L., and Schultz, P. G. (1994) *Proc. Natl. Acad. Sci. U.S.A. 91*, 2910−2914.
40. Nowak, M. W., Kearney, P. C., Sampson, J. R., Saks, M. E., Labarca, C. G., Silverman, S. K., Zhong, W., Thorson, J., Abelson, J. N., Davidson, N., Schultz, P. G., Dougherty, D. A., and Lester, H. A. (1995) *Science 268*, 439−442.
41. Mamaev, S. V., Laikhter, A. L., Arslan, T., and Hecht, S. M. (1996) *J. Am. Chem. Soc. 118*, 7243−7244.
42. Steward, L. E., Collins, C. S., Gilmore, M. A., Carlson, J. E., Ross, J. B. A., and Chamberlin, A. R. (1997) *J. Am. Chem. Soc. 119*, 6−11.
43. Karginov, V. A., Mamaev, S. V., An, H., Van Cleve, M. D., Hecht, S. M., Komatsoulis, G. A., and Abelson, J. N. (1997) *J. Am. Chem. Soc. 119*, 8166−8176.
44. Karginov, V. A., Mamaev, S. V., and Hecht, S. M. (1997) *Nucleic Acids Res. 25*, 3912−3916.
45. Arslan, T., Mamev, S. V., Mamaeva, N. V., and Hecht, S. M. (1997) *J. Am. Chem. Soc. 119*, 10877−10887.
46. Lodder, M., Golovine, S., and Hecht, S. M. (1997) *J. Org. Chem. 62*, 778−779.
47. Killian, J. A., Van Cleve, M. D., Shayo, Y. F., and Hecht, S. M. (1998) *J. Am. Chem. Soc. 120*, 3032−3042.
48. Short, G. F., III, Lodder, M., Laikhter, A. L., Arslan, T., and Hecht, S. M. (1999) *J. Am. Chem. Soc. 121*, 478−479.
49. Short, G. F., III, Golovine, S. Y., and Hecht, S. M. (1999) *Biochemistry 38*, 8808−8819.
50. Lodder, M., Crasto, C. F., Laikhter, A. L., An, H., Arslan, T., Karginov, V. A., and Hecht, S. M. (2000) *Can. J. Chem.* (in press).
51. Lesley, S. A., Brow, M. A. D., and Burgess, R. R. (1991) *J. Biol. Chem. 266*, 2632−2638.
52. Laemmli, U. K. (1970) *Nature 227*, 680−685.
53. Hyland, L. J., Tomaszek, T. A., Jr., and Meek, T. D. (1991) *Biochemistry 30*, 8454−8463.
54. Szeltner, Z., and Polgár, L. (1996) *J. Biol. Chem. 271*, 32180−32184.
55. Brooks, B. R., Bruccoleri, R. E., Olafson, B. D., States, D. J., Swaminathan, S., and Karplus, M. (1983) *J. Comput. Chem. 4*, 187−217.
56. Bhat, T. N., Baldwin, E. T., Liu, B., Cheng, Y. S., and Erickson, J. W. (1994) *Nat. Struct. Biol. 1*, 552−556.
57. Brünger, A. T., and Karplus, M. (1988) *Proteins 4*, 148−156.
58. Rykaert, J. P., Ciccotti, G., and Berendensen, H. J. C. (1977) *J. Comput. Phys. 23*, 327−341.
59. Louie, A., Ribeiro, N. S., Reid, B. R., and Jurnak, F. (1984) *J. Biol. Chem. 259*, 5010−5016.
60. Pettit, S. C., Simsic, J., Loeb, D. D., Everitt, L., Hutchison, C. A., III, and Swanstrom, R. (1991) *J. Biol. Chem. 266*, 14539−14547.
61. Babé, L. M., Pichuantes, S., and Craik, C. S. (1991) *Biochemistry 30*, 106−111.
62. Polgar, L. (1989) *Mechanisms of Protease Actions*, pp 157−182, CRC Press Inc., Boca Raton, FL.
63. Tang, J. (1971) *J. Biol. Chem. 246*, 4510−4517.
64. Meek, T. D., Dayton, B. D., Metcalf, B. W., Dreyer, G. B., Strickler, J. E., Gorniak, J. G., Rosenberg, M., Moore, M. L., Magaard, V. W., and Debouck, C. (1989) *Proc. Natl. Acad. Sci. U.S.A. 86*, 1841−1845.
65. Phylip, L. H., Richards, A. D., Kay, J., Konvalinka, J., Strop, P., Blaha, I., Velek, J., Kostaka, V., Ritchie, A. J., Broadhurst, A. V., Farmerie, W. G., Scarborough, P. E., and Dunn, B. M. (1990) *Biochem. Biophys. Res. Commun. 171*, 439−444.
66. Tozser, J., Weber, I. T., Gustchnia, A., Blaha, I., Copeland, T. D., Louis, J. M., and Oroszlan, S. (1992) *Biochemistry 31*, 4793−4800.

BI000214T